UC San Diego

UC San Diego Previously Published Works

Title

Differences in clinical features and mental health service use in bipolar disorder across the lifespan

Permalink

https://escholarship.org/uc/item/29m5r60q

Journal

American Journal of Geriatric Psychiatry, 13(4)

ISSN

1064-7481

Authors

Depp, Colin A
Lindamer, L A
Folsom, D P
et al.

Publication Date

2005-04-01

Peer reviewed

eScholarship.org Powered by the California Digital Library
University of California

A. García-García [1]*, S. García-Gil[2], F. Vilas[2]

Echo characters and recent sedimentary processes as indicated by high-resolution sub-bottom profiling in Ría de Vigo (NW Spain)

[1] Earth Sciences Dept. University of California Santa Cruz. CA 95064, USA.
[2] Dept. Geociencias Marinas y O. T. Universidad de Vigo. E-36200 Vigo, Spain.
* Corresponding author. Fax: +001 8314593074. E-mail address: agarcia@es.ucsc.edu

Abstract A detailed study of high-resolution (3.5 kHz) sub-bottom profiles reveals the presence of 17 different types of echo character (acoustic facies) in the recent sedimentary infill of the shallow Ría de Vigo (NW Spain). By correlating the echo-character with surface sediments, we have been able to infer the recent sediment dynamics in the ría seafloor, 60.5 % being related to modern depositional processes. In the outer area, where wave activity is strong, erosive and high-energy depositional processes dominate, whereas in the protected area of the inner ría the majority of recent processes are low-energy depositional, progradational and/or a combination of both.

Introduction

The most widely applied method for studying Quaternary sedimentary features and processes on continental rises is echo-character analysis (Damuth 1980). Since the early 1960s, high-resolution (3.5-12 kHz) echograms have been used extensively for this purpose. Correlation of echo-character analysis with current-meter data, sediment cores, and side-scan sonar imagery has been a highly successful method for understanding the distribution and origin of deep-sea bedforms (Poag and de Graciansky 1992).

The identification of acoustic facies relies on the sub-surface response to high-frequency seismic energy, in particular the observed echo duration, amplitude, and number of reflectors (Damuth 1975; Frappa and Duprat 1983). In addition, horizontal disposition and continuity of elementary echoes is also a characteristic of an acoustic facies. Finally, the ability to accurately define acoustic facies on the basis of echo character depends on the evolution of the seismic reflectors along and between individual survey lines (Frappa and Pujos 1994).

The acoustic energy returned by a given reflector depends initially on its differential acoustic impedance; that is, the impedance contrast between the units above and below the surface. Moreover, the energy reflected is a function of surface roughness and signal wavelength (Sheriff 1977). At 3.5 kHz, the wavelength for loose-grained surficial deposits is approximately 0.5 m (Frappa and Pujos 1994).

The study of high-resolution seismic sub-bottom profiler data (3.5 kHz) provides accurate information on the seabed's texture, microtopography, and erosive and depositional processes (Damuth 1980; Pratson and Laine 1989). This indirect technique has been widely used in deepwater environments (Damuth 1975; Johnson and Damuth 1979; Damuth 1980; Poag and de Graciansky 1992; Driscoll and Laine 1996; Howe et al. 1997; Pérez Fernández et al. 1997; Gilbert et al. 1998; Pudsey and Howe 1998; Lee et al. 1999; Gee et al. 1999; Sager et al. 1999; Wynn et al. 2000; Zaragosi et al. 2000; Droz et al. 2001). More recently, it has also been used for shallower marine areas (MacClennen 1989; Rey 1993; Reddy and Rao 1997; Yoon et al. 1997; Lobo and Hernández-Molina 1998; Frappa and Pujos 2000).

Although several studies have been conducted in the Galician rías, some focusing on their recent sediments (Fernández-Bastero et al. 1999; García et al. 2000; Rubio et al. 2000; Diz et al. 2001), only a few have targeted their Holocene sedimentary infill (Margalef 1956; Acosta 1984; Hernández-Molina et al. 1994; García-Gil et al. 1999a, 1999b; Vilas in press). The objective of the present study is to provide accurate information on the texture, microtopography, and erosive and depositional processes of the seabed of a ría environment through the detailed study of high-resolution sub-bottom profiler records.

Study area: Ría de Vigo

The Ría de Vigo (Fig. 1a) is located on the passive Atlantic margin of southwestern Galicia (NW Spain), the ría coast known as Rías Baixas. The Ría de Vigo's physiography presents a distinctive funnel shape, with an areal extent of 176.4 km^2. The Ría de Vigo trends at nearly right angles to the region's Paleozoic basement structure (Fig. 1b). Its basement comprises Paleozoic metamorphic and granitic rocks cut by NE-SW, NW-SE and N-S trending faults. The entire ría coast is possibly related to the post-Pyrenean extensional phase, during both the Oligocene and Miocene (García-Gil et al. 1999b).

The water depths within the Ría de Vigo range from 7 m in its inner part, to 53 m at the outer (southwest) entrance to the sea (Fig. 2a). The north entrance is shallow, with a max. depth of 30 m, with the deeper southern entrance to more than 50 m depth. The grain-size distribution of the present seafloor consists of mixed siliciclastic and skeletal gravels in both the outer area and the edges of the ria, whereas the central and inner parts of the ría are dominated by clay and silt with up to 10 % organic matter content (Vilas et al. 1995).

Methods

During the summer of 1991 a survey was conducted aboard R/V "*El Investigador*". A total of 640 km of seismic lines were acquired in the Ría de Vigo on a rectangular grid with lines spaced 66 to 550 m apart (Fig. 2b). These data were provided by a high-resolution seismic 1036 model ORE (3.5 kHz)

sub-bottom profiler, and an Atlas Deso 20 echosounder (33-210 kHz). Heave/swell correction was not applied during data acquisition. For navigation and position fixing, we used a Trimble 4000 RL Differential GPS station, combined with a transponder unit.

Sediment samples were collected using Van Veen and box core dredges during the Ministry of Public Works and Transportation (MOPT) cruise in 1991, and the University of Vigo (UVIGO) cruise in 1998. In the first ones, the particle size distribution of the sediments was measured using a combination of dry sieving for grain sizes larger than 63 mm and X-ray nephelometry for particles smaller than 63 mm (Micromeritics, Sedigraph 5100).

Grain-size distribution in the box core samples was determined by wet-sieving, with sieve columns ranging from 1 mm to 37 mm, spaced with a frequency of 1 phi (1000, 500, 250, 125, 62, 37 mm) when samples had a high value of medium sand. The average for the first 5 cm was the utilized value in this study. All this new data set was added to the available information of the recent sediments of Ría de Vigo (Vilas et al 1995).

Results

Echo-character (3.5 kHz) analysis

A detailed and specific classification of the different echo characters in the Ría de Vigo has been obtained following the methodology and classification proposed by Damuth (1980) and Pratson and Laine (1989), comparing the ría with similar echo types reported on other margins world-wide. A total of 17 echo characters have been identified, which were grouped into 9 different classes, depending on their acoustic responses.

CLASS 1: DISTINCT ECHO

This echo character, the most common in the Ría de Vigo area, discerns part of the sedimentary infill below the ría seafloor, due to its higher acoustic penetration (Fig. 3). Occasionally, the reflectors of the seismic units can be seen in detail, whereas in other cases, the only clear reflector is the basal reflector. There are several types of echoes within this class:

TYPE 1a: Transparent echo with visible seismic units and internal structure (Fig. 3a). When this echo appears, the seismic units, as well as their internal structure, can be observed on the seismic records. This echo character occupies 6.5 % of the surveyed area.

TYPE 1b: Transparent echo with visible seismic units but without internal structure (Fig. 3b). This echo type corresponds to 3.5 kHz echoes where seismic units, separated by discontinuities, can be

observed, but without any visible internal structure within the units. It represents 2.8 % of the surveyed area.

TYPE 1c: Transparent echo without visible seismic units but with a basal reflector (Fig. 3c). In this type of echo, the only strong reflector is the basal reflector and this is not always very distinct. This echo character is the most widely occurring echo type in the ría, occupying 25.2 % of the surveyed area.

TYPE 1d: Transparent echo with internal clinoforms (Fig. 3d). This echo type displays internal clinoforms which show progradational trends and covers an area of 2.8 % of the ría.

CLASS 2: INDISTINCT ECHO

These echoes show part of the sedimentary infill below the ría seafloor, but with more internal reflectivity than the previous class 1 (Fig. 4). Occasionally, the reflectors of the seismic units can be distinguished. There are two echo character types within this class:

TYPE 2a: Semi-transparent echo with visible seismic units (Fig. 4a). Echo character revealing seismic units, but generally without distinct internal structure. In the Ría de Vigo, this echo type appears only locally, representing a mere 1 % of the mapped area.

TYPE 2b: Semi-transparent echo without visible seismic units (Fig. 4b). This corresponds to an opaque seabed reflector which impedes the view of the seismic units. It represents the majority of class 2, and is more common in the Ría de Vigo area than type 2a, occupying 9.3 % of the surveyed area.

CLASS 3: HIGHLY REFLECTIVE ECHO (one type)

TYPE 3: This echo is highly reflective and opaque, with a very irregular and erosive seafloor (Fig. 5a). It occupies 8.4 % of the area.

CLASS 4: ECHO IN-STEP (one type)

TYPE 4: This echo character is opaque and hyperbolic with a high amplitude. It occurs very locally associated with a steep seafloor gradient (Fig. 5b), and represents only 1.4 % of the area.

CLASS 5: IRREGULAR ECHO (one type)

TYPE 5: This echo consists of irregular, hyperbolic and inclined reflectors, and appears very locally in the ría (Fig. 5c), representing a mere 0.5 % of the survey area.

CLASS 6: HYPERBOLIC ECHO

This class of echo is characterized by the presence of a hyperbolic geometry (Fig. 6) with less amplitude than the previous classes (4 and 5). Its areal extent is one of the largest that we found. Three different echo characters were present in this class:

TYPE 6a: Hyperbolic echo geometry with high amplitude (Fig. 6a). Echo character with a very open hyperbola, in which no internal reflector can be distinguished. It accounted for 1.4 % of the echoes found in the ría.

TYPE 6b: Hyperbolic echo geometry with variable amplitude (Fig. 6b). This echo is sometimes very reflective, and features tight hyperbolae. It represents the majority of class 6 echoes (23.4 %). This echo type is associated with a very rough seabed and is similar to echo “type I” of Pudsey and Howe (1998).

TYPE 6c: Hyperbolic echo geometry with low amplitude and hyperbolae below the seabed (Fig. 6c). Echo type with tight hyperbolae below the ría seabed, sometimes with their apexes tangential to the apparent seafloor. It is similar to echo “IVa” of Driscoll and Laine (1996). This echo represents only 0.9 % of the total.

CLASS 7: WAVY SEAFLOOR ECHOES

This echo character features wavy geometry, of variable amplitude with variable visibility of seismic units (Fig. 7). Several types can be found within this class:

TYPE 7a: Wavy seafloor, large and irregular. It appears in only 0.6 % of the total area.

TYPE 7b: Wavy seafloor, with or without internal structure, or with a channel shape. It appears in only 0.6 % of the area.

TYPE 7c: Wavy seabed with internal migrating or lenticular reflectors: echo with large, irregular amplitude waves, and reflectors migrated vertically. It accounts for 2 % of the echoes found in the ría.

CLASS 8: ECHO WITH ACOUSTIC BLANKING (one type)

TYPE 8: This echo, also of the most representative in the ría, is transparent to semi-transparent, with seismic units visible above the acoustic blanking (Fig. 8a). It represents 11.2 % of the total. Frappa and Pujos (1994) detected a similar echo in which the seismic units terminated abruptly and were replaced by a high-energy reflector.

CLASS 9: V-SHAPED ECHO (one type)

TYPE 9: This seabed is characterized by V-shaped depressions generally associated with the previous class 8 (Fig. 8b). It represents 2 % of the total echoes in the area, and is similar to the V-shaped depressions described by MacClennen (1989).

Echo-character mapping and ground truthing

The different echo-characters identified in the Ría de Vigo were compiled into an acoustic facies map (Fig. 9) by interpolating the acoustic classification (3.5 kHz) of the seabed and sub-bottom between the individual survey lines.

Class 1 echoes are located along the main axis of the ría. Type 1a occurs mainly in form of small patches in the inner and the central part of the outer ría. Type 1b is mainly located along the southern coast of the ría. Type 1c appears mostly in the central part of the outer ría, being the most representative echo type in the area. Type 1d occurs along the shallow edges of the outer ría.

Class 2 echoes occur along the northern and southern margin of the entrance of the outer ría, seaward of the Cíes Islands (type 2a). Type 2b occurs in isolated areas only.

The highly reflective echo of class 3 is located mainly in the northern entrance of the Ría de Vigo and locally along the southern coast of the ría. The echo in-step of class 4 is situated just east of the Cíes Islands and around some structural highs along the northern coast. The irregular echo of class 5 is rather rare and appears to be related to structural highs in the central zone.

The hyperbolic echoes of class 6 are located near the Cíes Islands and in nearshore areas mainly to the south and west of the outer ría where they are associated with basement outcrops. Type 6a is located along the northern coast of the inner ría. Type 6b occupies a larger area than type 6a and 6c, being restricted to the coastline of the outer ría, whereas type 6c was observed only along the southern coast of the outer ría.

The wavy seafloor associated with class 7 occurs in the north parts of the inner ría (Types 7a and 7b) and in a small bay in the southern area of the outer ría (Baiona).

Finally, acoustic blanking and V-shaped echoes (classes 8 and 9, respectively) appear along the central axis of both the inner and outer ría respectively, being associated with gassy sediments and gas seep features (pockmarks).

Since the map of recent sediment distribution in the ría (Fig. 10) shows six different lithologies, further sampling would be required to provide a more accurate characterization of every echo type and to re-evaluate the grain-size analyses associated with to the 17 echo types.

Discussion and Conclusions

Recent sedimentary processes

Taking into account our echo-character mapping (Fig. 9) as well as sediment lithology and recent sediment distribution in the area (Fig. 10), there is a clear correspondence between these lithologies and the 3.5 kHz echo responses (Table 1). This has previously been noted by Damuth (1975) who pointed out that limited sub-bottom penetration suggests relatively coarse grain sizes, whereas deep penetration suggests fine grain sizes.

Distinct echoes (class 1) appear where the seafloor is generally covered with muddy sediments (Fig. 10). The grain size of samples belonging to type 1a echoes corresponds to muds (Table 1). Being fine sediments, the acoustic response on these records is very distinct, and it is possible to distinguish relatively thin sediment layers and individual seismic units. Type 1b echoes correspond to muds containing some sand. The acoustic signal therefore has a lower penetration than in the case of type 1a. As a result, individual seismic units cannot be distinguished. Where the sediment is coarser, the echo comprises only a basal reflector because the coarse material does not allow the signal to penetrate deep enough (echo 1c). The last type in this class, echo 1d, is associated with medium sands and muds (Table 1). The progradational units constituting this echo character therefore have a sandy composition, the acoustic energy only penetrating a few meters.

Seafloor characterized by indistinct echoes (class 2) are composed of coarser sediments than in the case of class 1. As shown in table 1, the sediment of samples corresponding to echoes in class 2 is composed of sands. Type 2a comprises coarse-medium sands, giving poor penetration on the records. Sediments from type 2b are even coarser, being classified as coarse sands.

The highly reflective class 3 echoes generally correspond to schists and other rocks (Table 1). These echoes, located in the northern ría entrance and of several points in the south, are associated with metamorphic outcrops on the ría seafloor. These metamorphic rocks are the continuation of the outcrops on land.

The in-step echo (class 4) corresponds to sediment composed of muds and shell fragments. Its coarse composition explains the poor acoustic penetration. Another irregular echo type (type 5) is associated with muddy sediments, on account of which the irregular sub-bottom can be seen. This echo type is always located near basement outcrops.

The hyperbolic echo type 6a, which occurs in the northern area, corresponds to bioclastic sands and muddy sediments (Table 1). Due to the sandy component, the signal cannot penetrate much further than the seafloor. Type 6b is the typical echo character of irregular basement outcrops associated with granitic terrain also found on land. Type 6c represents the same rocky area as type 6b, but buried and covered by finer muddy material, as indicated in the sediments distribution of Vilas et al. (1995).

Wavy seafloor (class 7) is indicative of muddy sediments (Table 1). Type 7a comprises sediments containing some fine and medium sands which are responsible for the poor penetration. Type 7b consists of muddy sands which accounts for the poor penetration in the sediment infill. Type 7c corresponds to muds and sands. Where the mud content is high the penetration increases, although acoustic blanking may occur due to the presence of gas in the sediments (García-Gil et al. 2002).

Classes 8 and 9 are located in the central-inner parts of the Ría de Vigo, where the sediment is mainly mud (Table 1). These two classes of echoes indicate the existence of gas-charged sediment in the ría (García-García et al. 1999; García-Gil et al. 1999a, 2002; Vilas et al. 1999), which produces acoustic masking. Gas accumulations occur mainly along the central axis of the ría in two main gas fields and together these areas represent 12.6 km^2. The seafloor area affected by seeps is about 96km^2 of the whole Ría de Vigo area, being these V-shaped depressions originated because of fluids (gas) escaping from the seabed (García-Gil et al. 2002).

Implications

The combined mapping of echo-character and recent sediment distribution in the area enables us to produce a map showing recent sedimentary processes (Fig. 11). As indicated in Table 1, and following the terminology of Damuth (1980), all echoes types in class 1 would correspond to low-energy depositional processes, which in turn correspond to muddy sediments deposited in restricted areas where the hydrodynamic energy is low. Echoes in class 2 (types 2a and 2b) also indicate depositional processes but involve coarser sediments and are thus located in more exposed areas where the hydrodynamic energy is higher.

Two other depositional processes are called *progradational* and *gravitational* (Fig. 11). Progradational processes (types 1d and 6a) present a continuous echo with dipping sub-bottom reflectors. Gravitational processes are associated with slump deposits (type 5).

The association of mainly depositional and combined (depositional and erosional) processes produce the echo type 4. Sediments of this echo type are mostly composed of sand deposits which are to some degree affected by erosion.

Erosive processes characterize two different echo signals: types 3 and 7b. Type 3 echoes are present in places where there is a lack of sediment and the seafloor consists of metamorphic rock. Type 7b represents a channel-like depression, where erosion is noticeable (Fig. 7b).

Along the ría coast both erosive and depositional processes can be observed. This is the case with types 7a and 7c in class 7, which have a wavy or channeled seafloor displaying both erosive and depositional areas.

The presence of gas-charged sediments leads to the formation of gas seeps in the form of V-shaped depressions or pockmarks (type 9). Using the 3.5 kHz system, these features were restricted to the inner ría zone (Fig. 11). However, using other seismic instrumentation, evidence has also been found of gas pockets in the outer ría (García-García et al. 1999; Vilas et al. 1999; García-Gil et al. 2002).

Finally, in the outer ría, types 6b and 6c echoes are typical of places revealing acoustic basement. Type 6b is associated with granite outcrops, whereas in type 6c the basement is drapped by a thin layer of sediments.

On an areal basis, the mapped seafloor is dominated by depositional processes, in total covering 60.5 % (Fig. 11). Of this area, 45 % represents low-energy depositional processes (types 1a, 1b, 1c and 8), 10 % high-energy depositional processes (types 2a and 2b), 4 % progradational processes (types 1d and 6a), 0.5 % gravitational ones (type 5), and 1 % combined processes (type 4). Erosion occurs (types 3 and 7b) in 9 % of the total area, combined processes (types 7a and 7c) 4 %, and gas seeps (type 9) 2 %. Acoustic basement (types 6b and 6c) is exposed in 24.5% of the survey area.

Following the proposed zonation of ría environments (Vilas, 2003), the surveyed area corresponds to the marine domain (Table 2). Although muddy sediments with a high organic content dominate in the inner ría where dynamics are low, the outer ría is characterized by mixed siliciclastics and skeletal gravels indicative of higher energy. Escape processes are entirely restricted to the inner ría, as well as 45.3 % of low-energy depositional processes, 42.1 % of progradational ones, and 53.1 % of combined processes. By contrast, 100 % of the gravitational processes occur in the outer ría, as well as 95.3 % of basement outcrops, 76.6 % of erosive processes, 81% of high-energy of depositional processes, and 90.6 % of depositional/combined processes.

All of the available evidence points towards a good correlation between the proposed zonation of ría environments and recent processes observed in this particular ría. In the outer ría, where wave action is strong, erosive processes as well as high-energy depositional processes occur. In the protected area of the inner ría, the majority of recent processes are low-energy depositional, progradational, and combined processes.

Acknowledgements

This work has been supported by a post-doc research grant EX2002-0627 by the MECD and Spanish Projects PGIDT00PXI30105PR and MAR REN2000-1102. The authors thank Paula Diz of the University of Vigo for the box core data. The authors also thank the useful and constructive comments of two anonymous referees. We thank Dr. Daniel Orange for his review of the previous draft. The present paper is contribution 257 to the EX-1 Group of the University of Vigo.

References

Acosta J (1984) Occurrence of acoustic masking in sediments in two areas of the continental shelf of Spain: Ría de Muros (NW) and Gulf of Cadiz (SW). Mar Geol 58:427-434

Damuth JE (1975) Echo character of western equatorial Atlantic floor and its relationship to the dispersal and the distribution of the terrigeneous sediments. Mar Geol 18:17-45

Damuth JE (1980) Use of high-frequency (3.5 kHz-12 kHz) echograms in the study of near-bottom sedimentation processes in the deep-sea: a review. Mar Geol 38:51-75.

Diz P, Francés G, Vilas F (2001) Microhabitats of benthic foraminifera in the Ría de Vigo and their use in the paleoecological interpretation. Cuad Geol Iber 26:157-177

Driscoll NW, Laine, EP (1996) Abyssal current influence on the southwest Bermuda Rise and surrounding region. Mar Geol 130:231-263

Droz L, Kergoat R, Cochonat P, Berné S (2001) Recent sedimentary events in the western Gulf of Lions (Western Mediterranean). Mar Geol 176:23-37

Fernández-Bastero S, Alejo I, Nombela MA, García-Gil S, Francés G, Rubio B, Pérez-Arlucea M, Jiménez R, Rey D, Bernabeu A, Pazos O, Gago-Duport L, Vilas F, Santos A (1999) Chemical factors controlling the steady-state distribution of mixed carbonate-siliciclastic sediments in Bayona Bay (northwest Spain). Bol Inst Esp Oceanogr 15 (1-4):289-302

Frappa M, Duprat M (1983) Relation entre la réponse acoustique (5 kHz) et la nature lithologique des fonds marins. Mar Geophys Res 5:405-419

Frappa M, Pujos M (1994) Late Quaternary evolution of the French Guiana continental shelf: evidence from 3.5 kHz data. Mar Geol 121:231-245

García T, Velo A, Fernández-Bastero S, Alejo I, Gago-Duport L, Santos A, Vilas F (2000) Coupling of reaction-transport in mixed carbonated-siliciclastic sediments: Ría de Vigo and Baiona Bay. Jour Iber Geol 26:249-269

García-García A, García-Gil S, Vilas F (1999) A Seeping Seafloor in a Ría Environment: Ría de Vigo (NW Spain). Environ Geol 38 (4):296-300

García-Gil S, García-García A, Durán R, Vilas F (2000a) High-Resolution Seismic Stratigraphy of the Rías Baixas: Pontevedra and Vigo (NW Spain). Jour Iber Geol 26:217-231

García-Gil S, García-García A, Vilas F (1999a) Identificación Sísmico-acústica de las Diferentes Formas de Aparición de Gas en los Sedimentos de la Ría de Vigo (NO España). Rev Soc Geol España 12 (2):301-307

García-Gil S, Vilas F, García-García A (2000b) High-Resolution Seismic Analysis of the Würm Unconformity Surface in the Ría de Vigo (NW Spain). Proc. 3rd Symp Iberian Atlantic Cont Margin, Faro, Portugal, 25-27 Sept, University of Algarve, pp 45-46.

García-Gil S, Vilas F, García-García A (2002) Shallow Gas Features in Incised-valley Fills (Vigo ría, NW Spain). In: Judd, A., Curzi, P. (Eds.), Shallow Gas Studies Spec Issue Cont Shelf Res 22:2303-2315

García-Gil S, Vilas F, Muñoz A, Acosta J, Uchupi E (1999b) Quaternary Sedimentation in the Ría de Pontevedra (Galicia), Northwest Spain. Jour Coast Res 15 (4):1083-1090

Gee MJR, Masson DG, Watts AB, Allen, PA (1999) The Saharan debris flow: an insight into the mechanics of long runout submarine debris flows. Sedimentology 46:317-335

Gilbert IM, Pudsey CJ, Murray JW (1998) A sediment record of cyclic bottom-current variability from the northwest Weddell Sea. Sed Geol 115 (1-4):185-214

Hernández-Molina FJ, Somoza L, Rey J, Pomar L (1994) Late Pleistocene-Holocene sediments on the Spanish continental shelves: Model for very high resolution sequence stratigraphy. Mar Geol 120:129-174

Howe JA, Pudsey CJ, Cunningham AP (1997) Pliocene-Holocene contourite deposition under the Antarctic Circumpolar Current, Western Falkland trough, South Atlantic. Mar Geol 138 (1-2):27-50

Johnson DA, Damuth JE (1979) Deep thermohaline flow and current-controlled sedimentation in the Almirante passage: western Indian Ocean. Mar Geol 33:1-44

Lee SH, Chough SK, Back GG, Kim YB, Sung BS (1999) Gradual downslope change in high-resolution acoustic characters and geometry of large-scale submarine debris lobes in Ulleung Basin, East Sea (Sea of Japan), Korea. Geo-Mar Lett 19:254-261

Lobo FJ, Hernández-Molina, FJ (1998) Echo-character analysis as a useful tool for recent sedimentary processes determination on the continental shelf environment. 15th Int. Sediment Congress, Alicante, Spain, 12-17 April, University of Alicante, pp 507-508

MacClennen CE (1989) Microtopography and surficial sediment patterns in the central Gulf of Maine: a 3.5 kHz survey and interpretation. Mar Geol 89:69-85

Margalef R (1956) Paleoecología postglacial de la Ría de Vigo. Inv Pesq V:89-112

Pérez-Fernández LM, Rodero J, Lobo FJ, Hernández-Molina FJ, Maldonado A (1997) Caracterización de procesos deposicionales en el talud continental del sector meridional del Golfo de Cádiz (SW España). Proc. 2nd Symp Atlantic Iberian Cont Margin, Cadiz, Spain, 17-20 Sept, University of Cadiz, pp 129-130

Poag CW, de Graciansky PC (1992) Geologic Evolution of Continental Rises: A Circum-Atlantic Perspective. In: Poag, C. W. and de Graciansky, P. C. (Eds.) Geologic Evolution of Atlantic Continental Rises, Kluwer Academic Publishers, Dordrecht:347-368

Pratson LF, Laine EP (1989) The relative importance of gravity-induced versus current-controlled sedimentation during the Quaternary along the mideast U.S. outer continental margin revealed by 3.5 kHz echo character. Mar Geol 89:87-126

Pudsey CJ, Howe JA (1998) Quaternary history of the Antarctic Circumpolar Current: evidence from the Scotia Sea. Mar Geol 148:83-112

Reddy DR, Rao TS (1997) Echo characters of the continental margin, western Bay of Bengal, India. Mar Geol 140:201-217

Rey J (1993) Relación morfosedimentaria entre la plataforma continental de Galicia y las Rías Bajas y su evolución durante el Cuaternario. Public Espec Inst Esp Oceanogr 17, pp 1-232

Rubio B, Nombela MA, Vilas F (2000) Geochemistry of major and trace elements in sediments of the Ría de Vigo (NW Spain): an assessment of metal pollution. Mar Poll Bull 40 (11):968-980

Rubio H, Abril Hurtado J, García Salinas F, Corretge LG, Floor P, Zapartiel JM (1981) Hoja geológica núm. 223 (Vigo). Mapa Geológico de España E. 1:50.000. IGME, Madrid

Sager WW, Lee CS, Macdonald IR, Schroeder WW (1999) High-frequency near-bottom acoustic reflection signatures of hydrocarbon seeps on the Northern Gulf of Mexico continental slope. Geo-Mar Lett 18:267-276

Sheriff RE (1977) Limitations on resolution of seismic reflections geologic detail derivable from them. In: Seismic Stratigraphy-Application to Hydrocarbon Exploration. AAPG Mem. 26:3-14

Vilas F (2003) Rias and Tidal-Sea Estuaries. Chapter 2.6 Coastal Zone and Estuaries. Unesco-EOLSS (in press).

Vilas F, García-Gil S, García-García A (1999) Shallow Gas in Incised-valley Fills of the Ría de Vigo, NW Spain. EOS, Transactions (80) 46:557

Vilas F, Nombela MA, García-Gil E, García-Gil S, Alejo I, Rubio B, Pazos O (1995) Mapa de distribución de los sedimentos del fondo de la Ría de Vigo. Conselleria de Pesca, Marisqueo y Acuicultura, Xunta de Galicia

Wynn RB, Masson DG, Stow DAV, Weaver PPE (2000) The Northwest African slope apron: a modern analogue for deep-water systems with complex seafloor topography. Mar Petrol Geol 17:253-265

Yoon HI, Han MW, Park B-K, Oh J-K, Chang S-K (1997) Glaciomarine sedimentation and palaeo-glacial setting of Maxwell Bay and its tributary embayment, Marian Cove, South Shetland Islands, West Antarctica. Mar Geol 140:265-282

Zaragosi S, Auffret GA, Faugères J-C, Garlan T, Pujol C, Cortijo E (2000) Physiography and recent sediment distribution of the Celtic Deep-Sea Fan, Bay of Biscay. Mar Geol 169:207-237

Table Captions

Table 1. Echo character types in the Ría de Vigo, seismic characteristics, and correspondence to lithology. Inferred recent sedimentary processes are also shown.

Table 2. Zonation of a ría environment, taking into account bottom morphology, sedimentary facies and dynamics (modified from Vilas, 2003). Note that the surveyed area would correspond only to the marine domain.

Figure Captions

Figure 1. (a) Geographical setting of the Ría de Vigo, located on the NW coast of Spain; (b) geological map of the ria: (1) Quaternary sediments, (2) metasediments, (3) paragneis, (4) orthogneis, and (5) granites. Continuous lines represent mechanical contacts, and dashed lines represent faults, anticlines and synclines. Modified from Rubio et al. 1981.

Figure 2. (a) The bathymetry of the Ría de Vigo. Bathymetric contours at 2 m intervals. The inner part presents a central channel, where it attains its maximum depth. In the southern entrance, bathymetry is deepest. (b) Survey tracklines in the area, with figure locations represented as thick lines above the seismic survey.

Figure 3. Examples of 3.5 kHz seismic lines showing the four different echo character types of class 1 (distinct echoes): (a) type 1a, (b) type 1b, (c) type 1c, (d) type 1d. See figure 2b for location of the seismic lines. Undulating seafloor reflector due to superimposed waves (swell).

Figure 4. Examples of 3.5 kHz seismic lines showing the two different echo character types of class 2 (indistinct echoes): (a) type 2a, (b) type 2b. See figure 2b for location of the seismic lines. Undulating seafloor reflector due to superimposed waves (swell).

Figure 5. Examples of 3.5 kHz seismic lines showing several classes of echoes: (a) type 3: highly reflective echo; (b) type 4: in-step echo; and (c) type 5: irregular echo. See figure 2b for location of the seismic lines. Undulating seafloor reflector due to superimposed waves (swell).

Figure 6. Examples of 3.5 kHz seismic lines showing the three different echo character types of class 6 (hyperbolic echoes): (a) type 6a, (b) type 6b, (c) type 6c. See figure 2b for location of the seismic lines.

Figure 7. Examples of 3.5 kHz seismic lines showing the three different echo character types of class 7 (wavy seafloor): (a) type 7a, (b) type 7b, (c) type 7c. See figure 2b for location of the seismic lines.

Figure 8. Examples of 3.5 kHz seismic lines showing: (a) type 8: echo with acoustic blanking; (b) type 9: V-shaped echo (pockmarks). See figure 2b for location of the seismic lines.

Figure 9. Acoustic facies map based on echo-character mapping of the 17 different echoes characters found in the ría: (1a) transparent echo with visible seismic units and internal structure; (1b) transparent echo with visible seismic units but without internal structure; (1c) transparent echo without visible seismic units, with basal reflector; (1d) transparent echo with internal clinoforms; (2a) semitransparent echo with visible seismic units; (2b) semitransparent echo without visible seismic units; (3) highly reflective echo; (4) echo in-step; (5) irregular echo; (6a) hyperbolic echo geometry with high amplitude; (6b) hyperbolic echo geometry with variable amplitude; (6c) hyperbolic echo geometry with low amplitude and hyperbolae below the seabed; (7a) wavy echo, large and irregular; (7b) wavy echo with wavy shape, with and without internal structure, or channel-shaped; (7c) wavy echo with internal migrating reflectors, with lenses; (8) echo with acoustic blanking; (9) V-shaped echo.

Figure 10. Distribution of the recent sediments in the Ría de Vigo seafloor (modified from Vilas et al. 1995). Crosses indicate Van Veen sample locations. “BC” crosses indicate a box core sample.

Figure 11. (a) The inferred recent sedimentary processes as distributed in the Ría de Vigo; (b) Percentage occurrence of various recent processes in the ría. In total, 60.5 % of the surface area of the Ría de Vigo is characterized by depositional processes, 9 % by erosive processes, and 25 % by acoustic basement.

Table 1

Echo character classes	Echo character types	Seismic character	Sample number	Description	Lithology (Vilas et al. 1995)	Inferred sedimentary processes
1. Distinct	Type 1a	Visible seismic units and internal structure	41, 472, 474, 476	Mud	Muds, sands	Low-energy depositional
	Type 1b	Visible seismic units without internal structure	29, 173, 608, 609, 611	Mud/bioclastic sands	Muds, sands	
	Type 1c	No visible seismic units, with one basal reflector	12, 18, 26, 776, 777	Muds/sandy muds	muds and sands	
	Type 1d	Internal clinoforms	469, 470	Medium sand/bioclastic sands	Sands and muds	Depositional progadational
2. Indistinct	Type 2a	Visible seismic units	130, 657	Algae/Coarse-medium sands	Sands	High-energy depositional
	Type 2b	No visible seismic units	3, 8, 9, 118, 827	Sands	Sands	
3. Highly reflective	Type 3	Opaque with irregular limit	1, 89, 91, 93, 244, 245, 246, 247	Rocks, schists	Sands	Erosive
4. Echo in step	Type 4	Hyperbolic, high amplitude, opaque	4, 53, 628	Mud/shell fragments	Muddy/gravel sands	Depositional/combined
5. Irregular	Type 5	Irregular	621	Mud	Muds	Depositional gravitational
6. Hyperbolic	Type 6a	High-amplitude	57, 679	Bioclastic sands/mud	Sand-gravel-mud	Depositional progradational
	Type 6b	Variable amplitude	20, 23, 799, 888, 1060, 1062	Rocks, shell fragments	-	
	Type 6c	Low-amplitude, with hyperbolae below the seabed	-	-	Muddy sands	Acoustic basement
7. Wavy	Type 7a	Big and irregular	798	Mud with fine-medium and bioclastic sands	Gravel/sandy muds	Combined (erosive and depositional)
	Type 7b	Channel-shaped	174, 175	Mud	Sands	Erosive
	Type 7c	With migrated infradepositional reflectors	45	Muds with sands	Sandy muds	Combined (erosive and depositional)
8. With acoustic blanking	Type 8	Acoustic masking	7, 39, 161, 167	Mud	Mud	Low-energy depositional
9. V-shaped	Type 9	“V” shape	10, 156	Mud	Mud	Gas escaping

Table 2

			Control	Morphology	Sedimentary facies	Dynamics
Ría environment	Estuary domain		Fluvial	Meandering channel, sandy levees, muddy sand flats and crevasse-splay deposits, roots, plant fragments	Coarse fluvial sand and gravel with no tidal structures and silty-clay lenses	Unidirectional water movement. Fluvial sediment source
			Tidal	Tidal estuarine sand bars and point bars, intertidal mud flats and salt marshes. Estuarine muds with isolated sand bodies	Channels with medium-grained ripples and cross-bedded sand. Masive muds with sand lenses and clay laminae	Intermitent dominance of fluvial-tidal Influence and changing water velocities. Sand movement in the fluvial-tidal zone. Bidirectional water and sand movement in the estuarine zone
	Marine domain	Inner ría	Tidal influence	Low-regime flat beds at the bottom. Small salt marshes and intertidal sandy-mud-flats, and sandy beaches to the flanks	Dominance of muds and fine sands. Low content in carbonates and high content in organic matter	Tide influence and weak waves. Bidirectional water movement. Local fluvial inputs. Low tidal velocities for sand movements
		Outer ría	Wave-dominated and tidal influence	Low-regime flat beds and low-relief sand bars at the bottom. Sandy beaches and small beach-barriers at the banks	Bottom: mixed siliciclastic and skeletal gravels with sandy or muddy component. Shoreline: coarser sands grading into clean skeletal carbonates sands. Low content in organic matter	Bidirectional water movement. Wave-dominated and tidal influence. Upwelling influence and local fluvial inputs

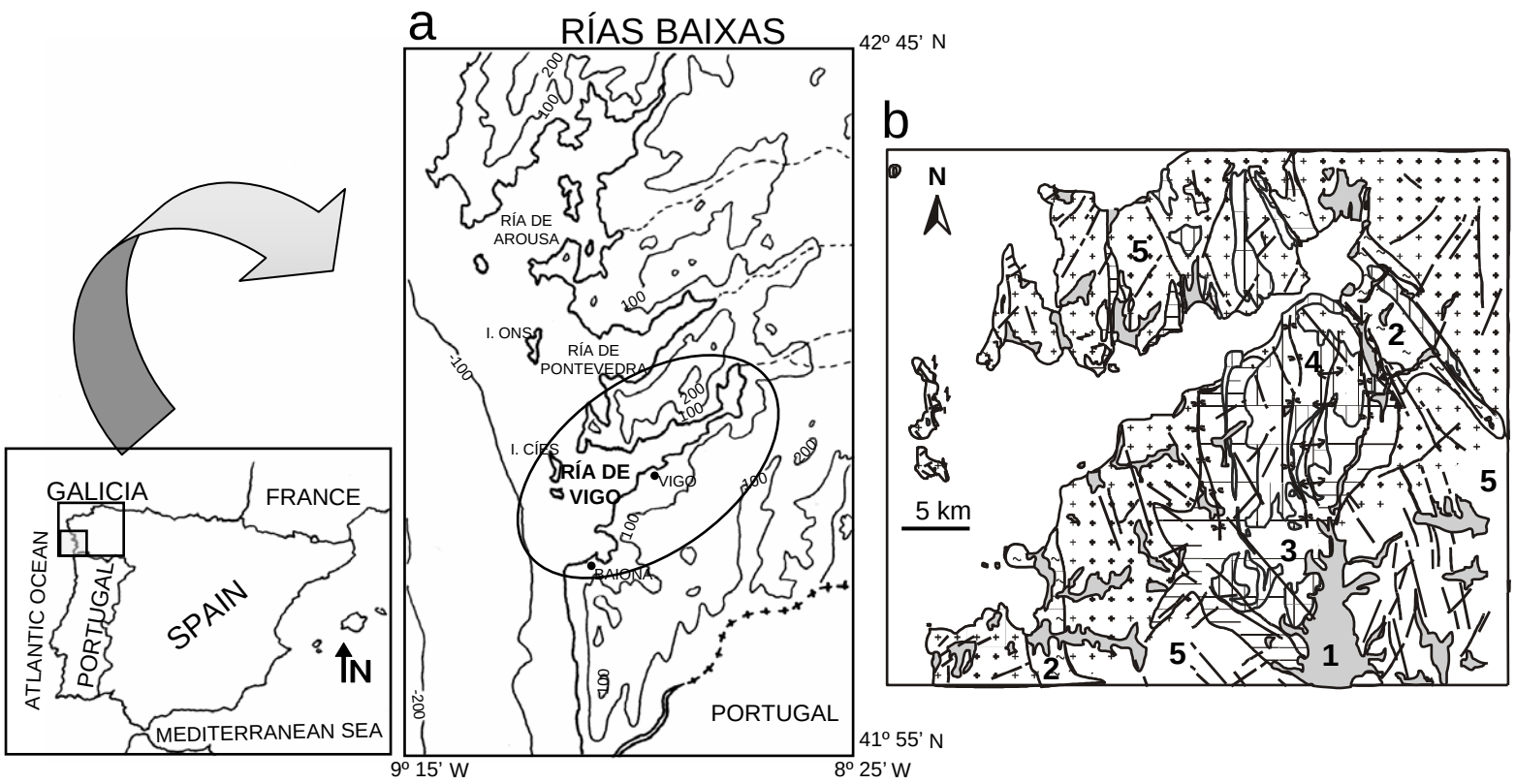
a
RÍAS BAIXAS
42º 45' N
41º 55' N
9º 15' W
8º 25' W
RÍA DE AROUSA
I. ONS
RÍA DE PONTEVEDRA
I. CÍES
RÍA DE VIGO
VIGO
BAIONA
PORTUGAL
-200
-100
100
200
GALICIA
FRANCE
SPAIN
PORTUGAL
ATLANTIC OCEAN
MEDITERRANEAN SEA
N
b
N
5 km
1
2
3
4
5

Figure 1

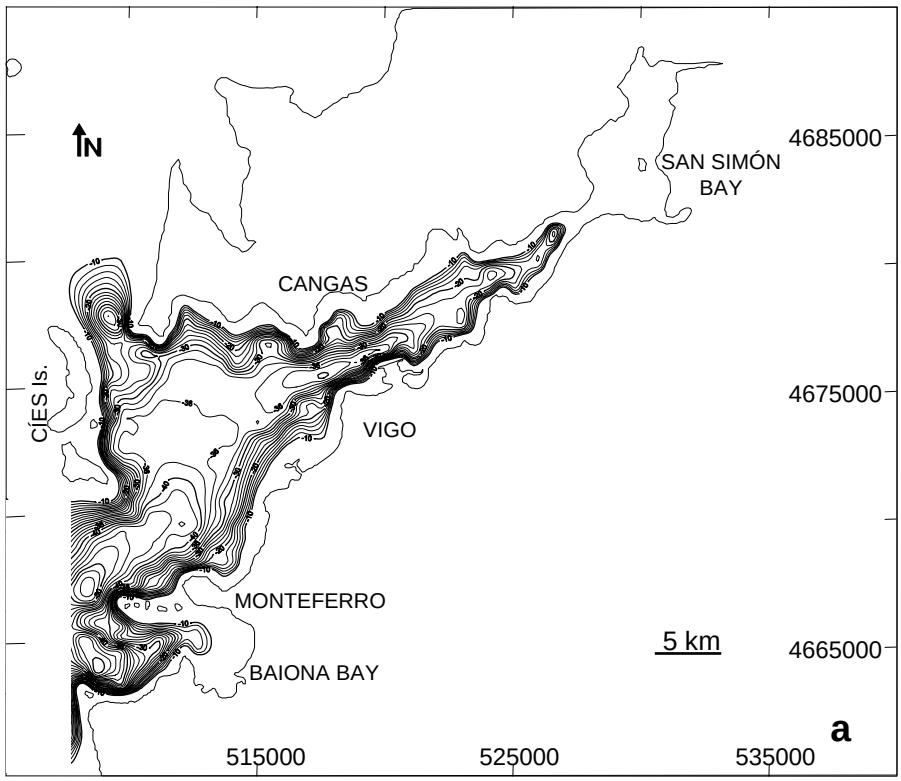
N
SAN SIMÓN
BAY
CANGAS
CÍES Is.
VIGO
MONTEFERRO
BAIONA BAY
5 km
a
4685000
4675000
4665000
515000
525000
535000

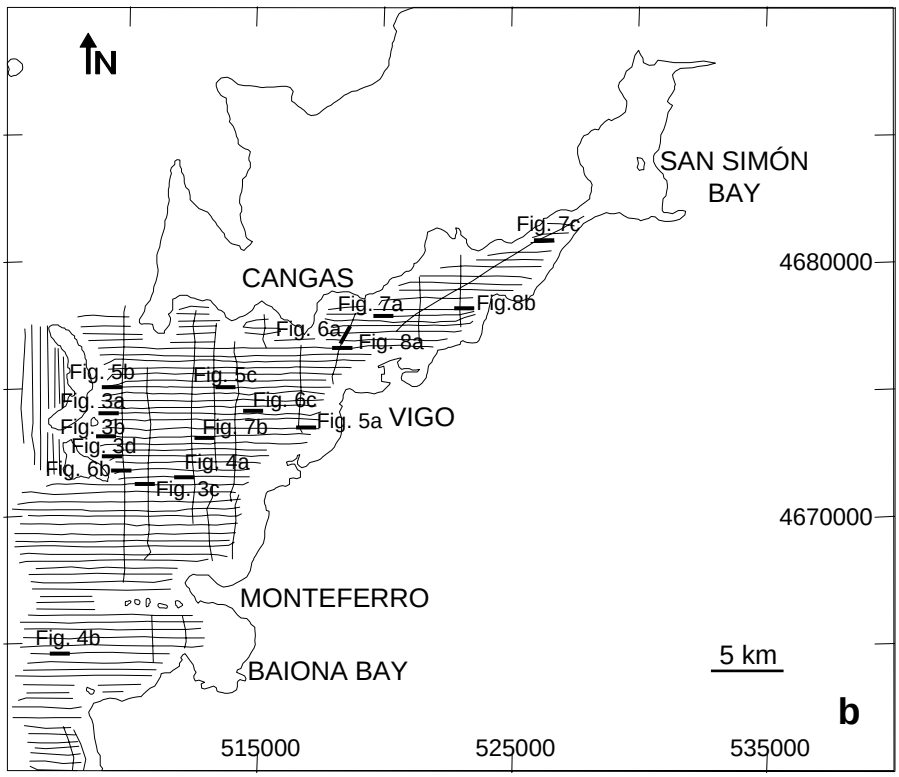
N
SAN SIMÓN
BAY
Fig. 7c
CANGAS
Fig. 7a
Fig.8b
Fig. 6a
Fig. 8a
Fig. 5b
Fig. 5c
Fig. 3a
Fig. 6c
Fig. 3b
Fig. 7b
Fig. 5a
VIGO
Fig. 3d
Fig. 6b
Fig. 4a
Fig. 3c
MONTEFERRO
Fig. 4b
BAIONA BAY
5 km
b
4680000
4670000
515000
525000
535000

Figure 2

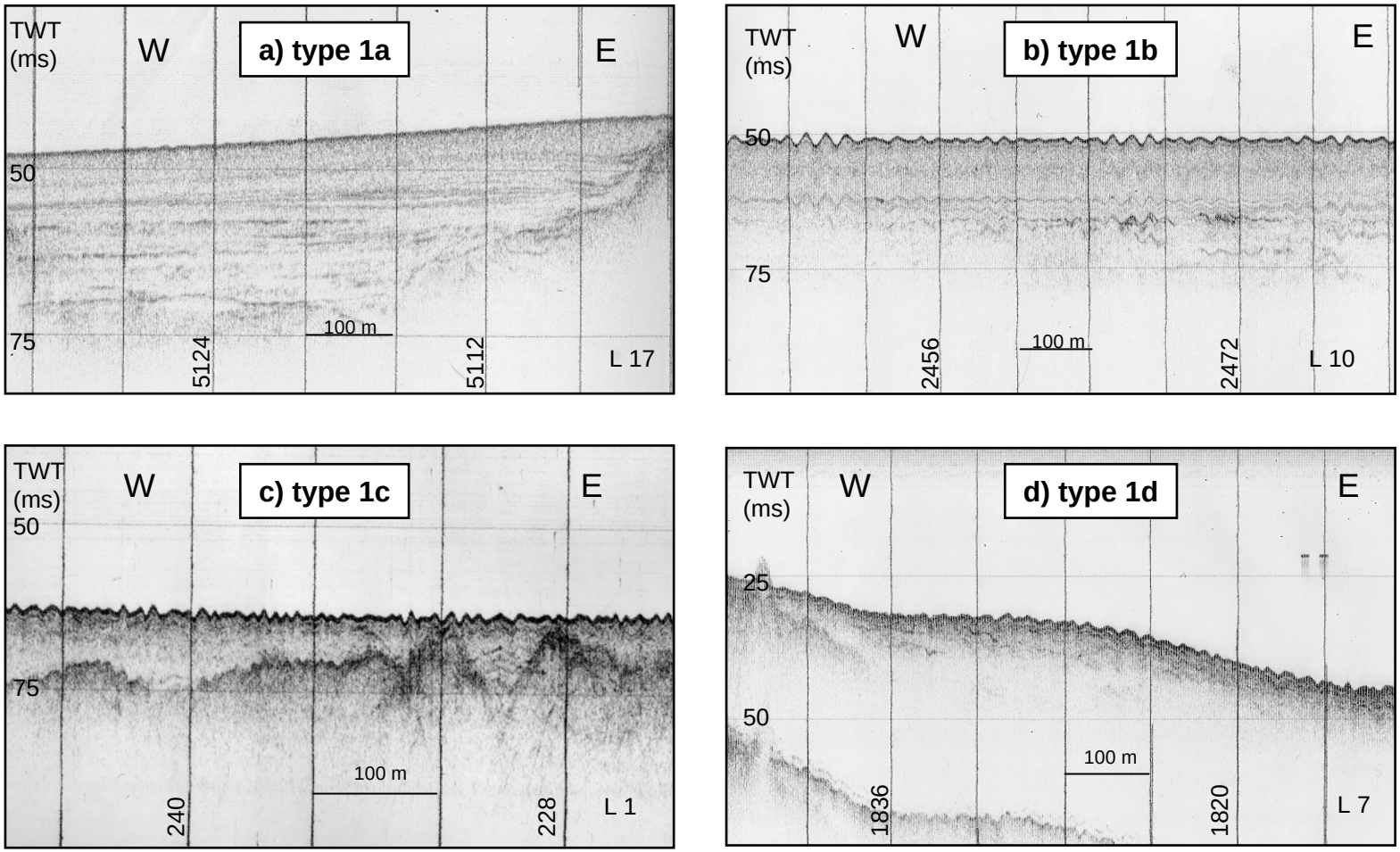
TWT
(ms)
W
a) type 1a
E
50
75
5124
100 m
5112
L 17
TWT
(ms)
W
b) type 1b
E
50
75
2456
100 m
2472
L 10
TWT
(ms)
50
W
c) type 1c
E
75
240
100 m
228
L 1
TWT
(ms)
W
d) type 1d
E
25
50
1836
100 m
1820
L 7

Figure 3

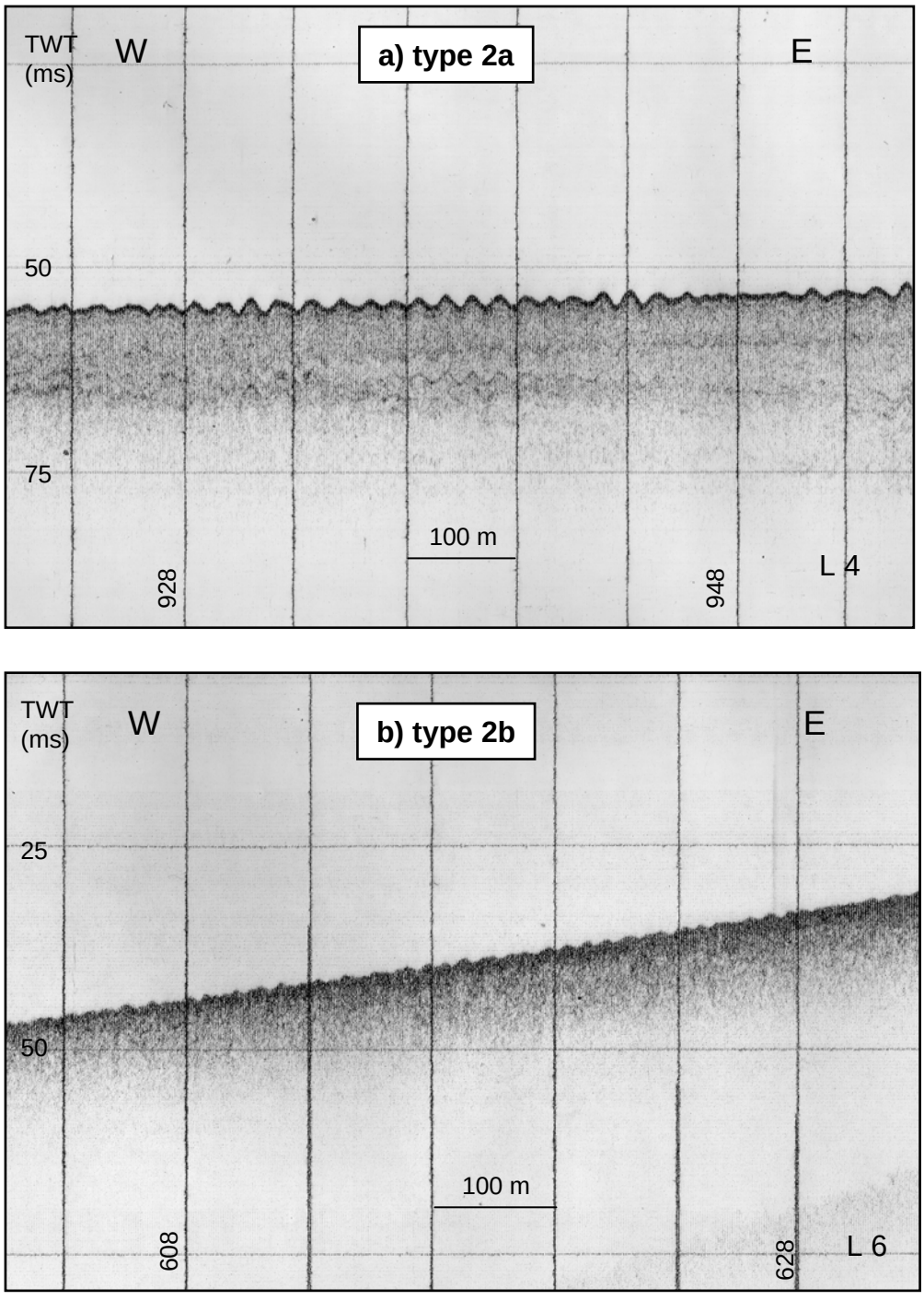
TWT
(ms)
W
a) type 2a
E
50
75
100 m
928
948
L 4
TWT
(ms)
W
b) type 2b
E
25
50
100 m
608
628
L 6

Figure 4

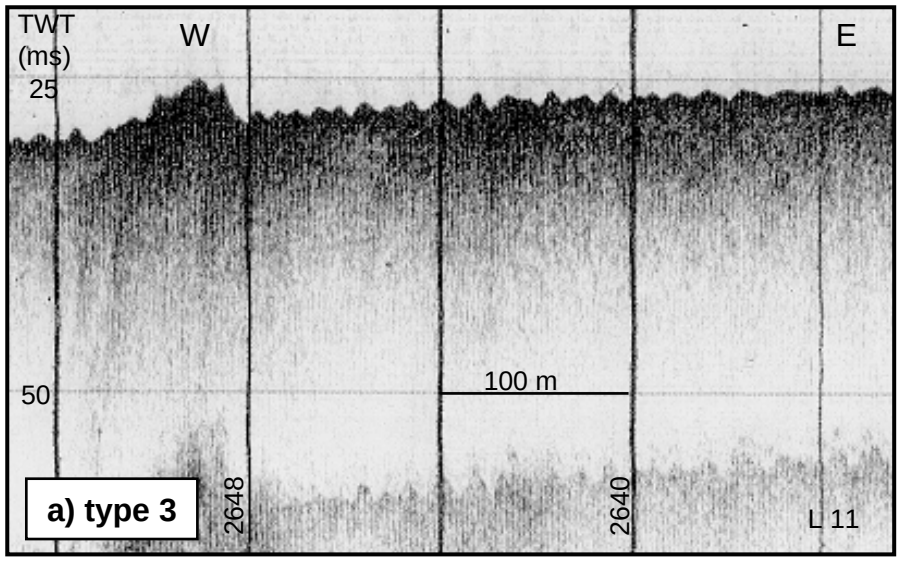
TWT
(m$)
W
E
25
50
100 m
a) type 3
2648
2640
L 11

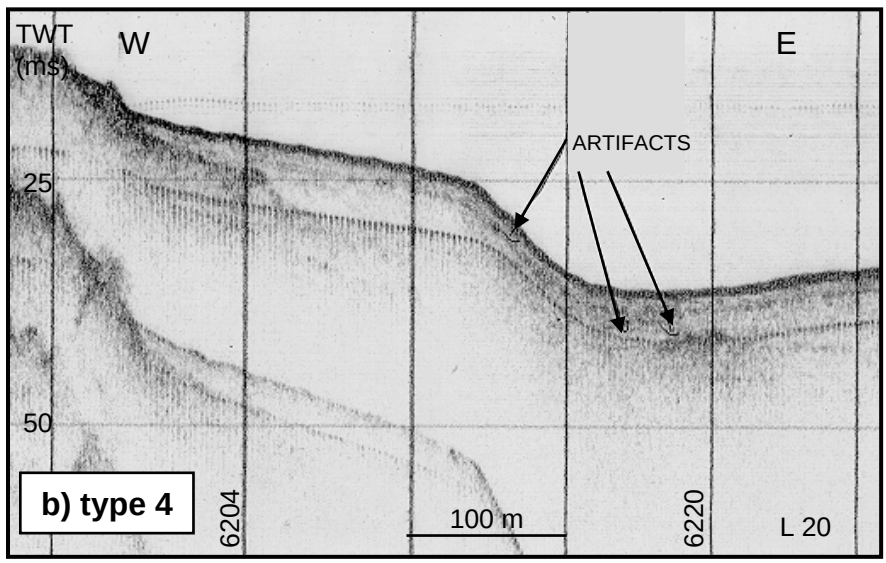
TWT
(m$)
W
E
ARTIFACTS
25
50
b) type 4
6204
100 m
6220
L 20

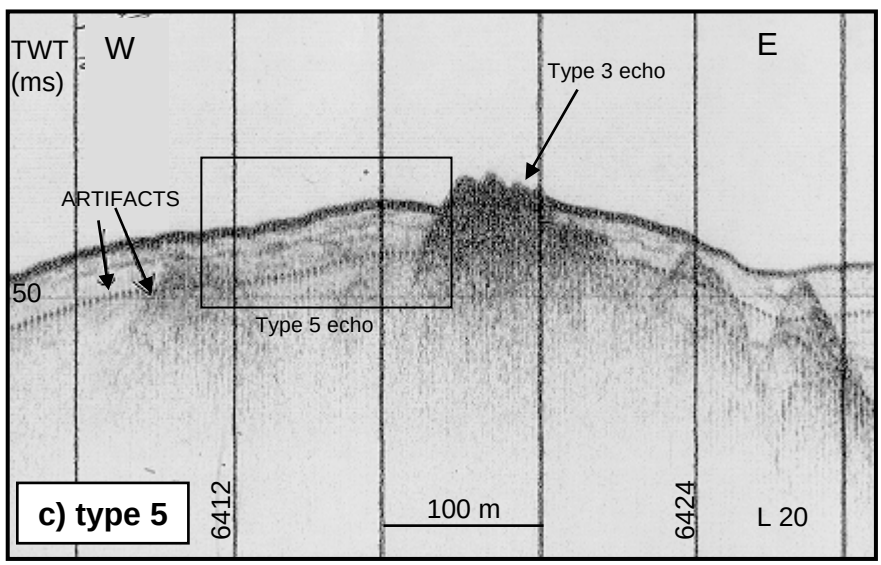
TWT
(ms)
W
E
Type 3 echo
ARTIFACTS
50
Type 5 echo
c) type 5
6412
100 m
6424
L 20

Figure 5

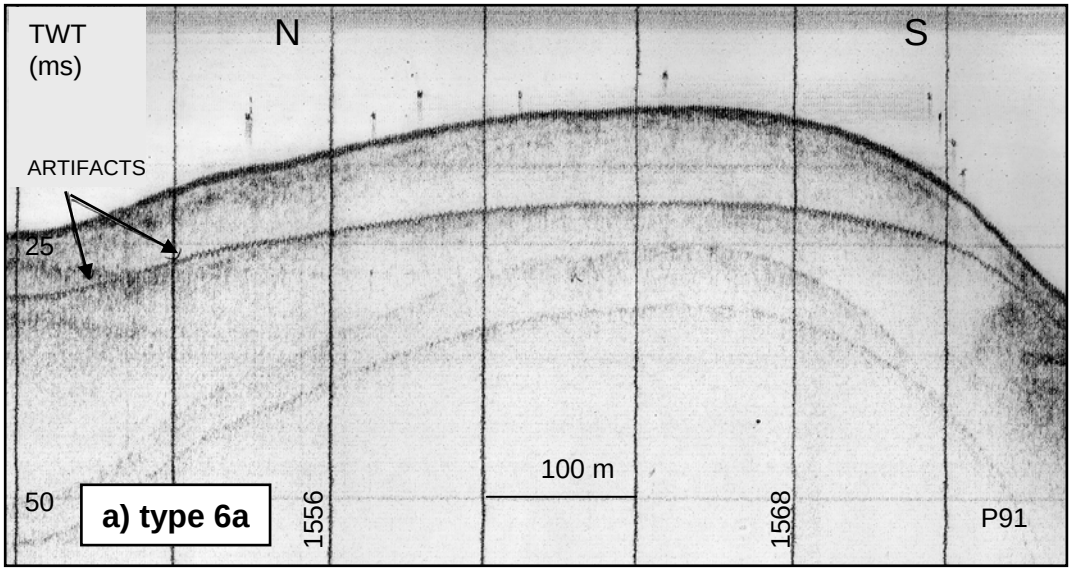
TWT
(ms)
N
S
ARTIFACTS
25
50
a) type 6a
1556
100 m
1568
P91

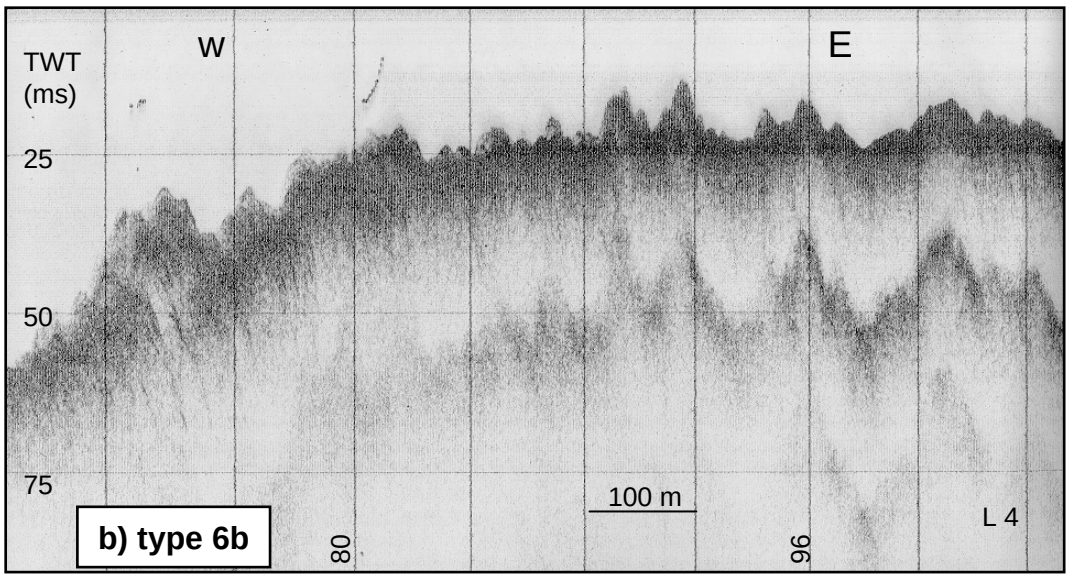
TWT
(ms)
W
E
25
50
75
b) type 6b
80
100 m
96
L 4

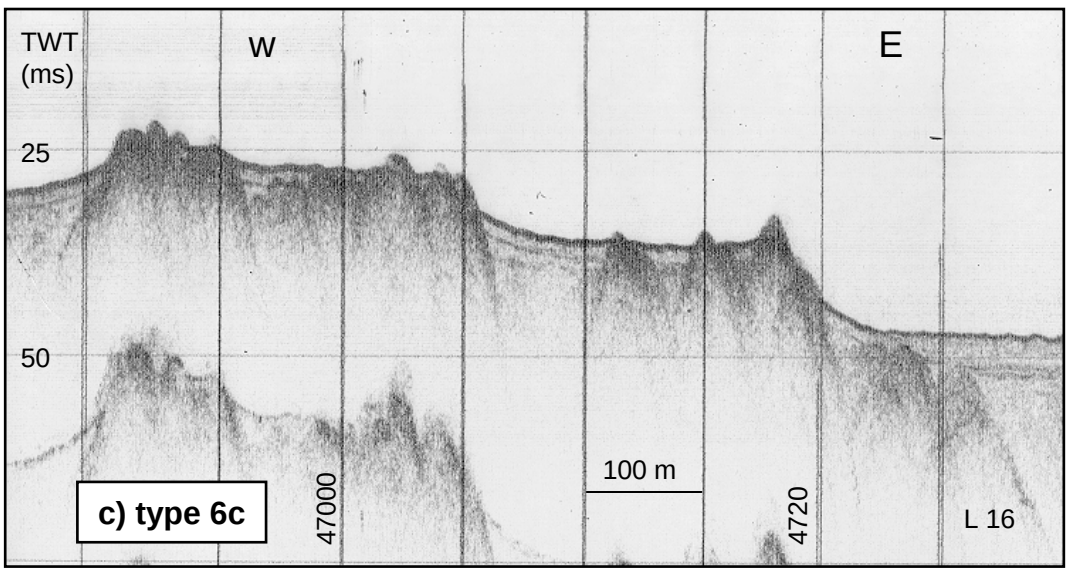
TWT
(ms)
W
E
25
50
c) type 6c
47000
100 m
4720
L 16

Figure 6

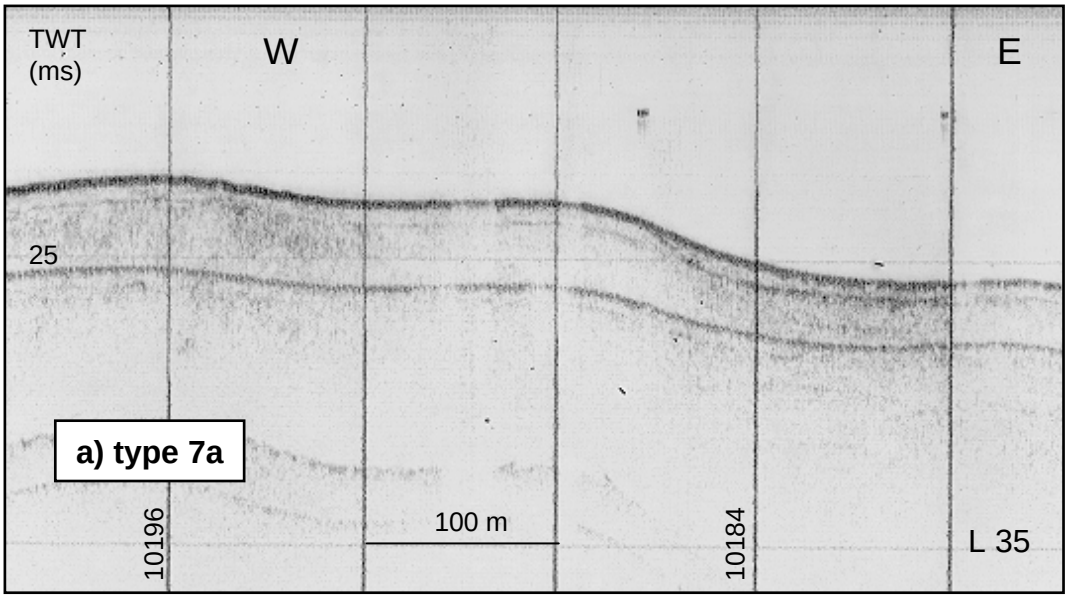
TWT
(ms)
W
E
25
a) type 7a
10196
100 m
10184
L 35

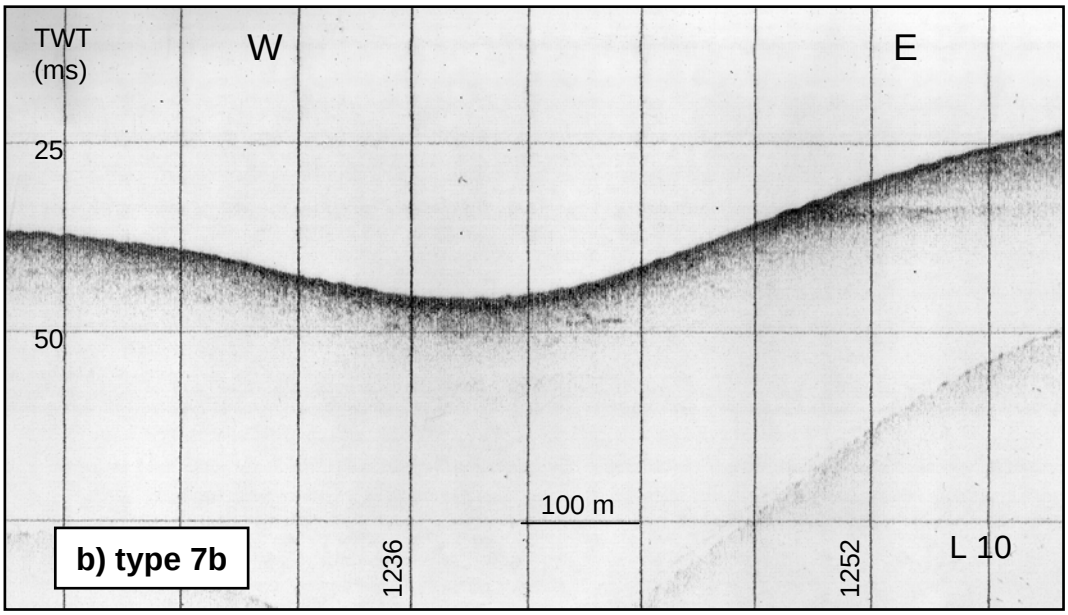
TWT
(ms)
W
E
25
50
100 m
b) type 7b
1236
1252
L 10

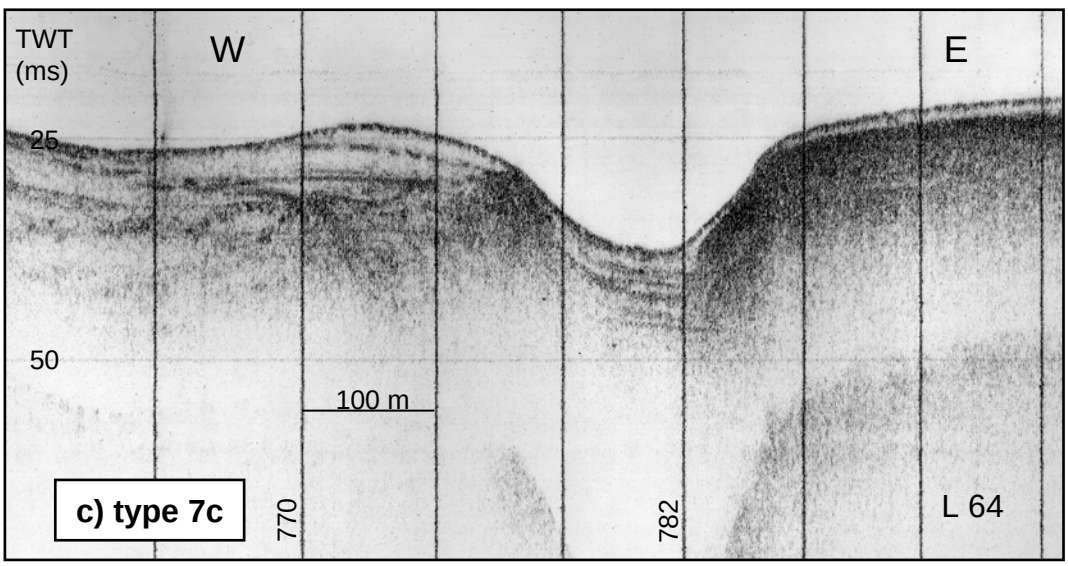
TWT
(ms)
W
E
25
50
100 m
c) type 7c
770
782
L 64

Figure 7

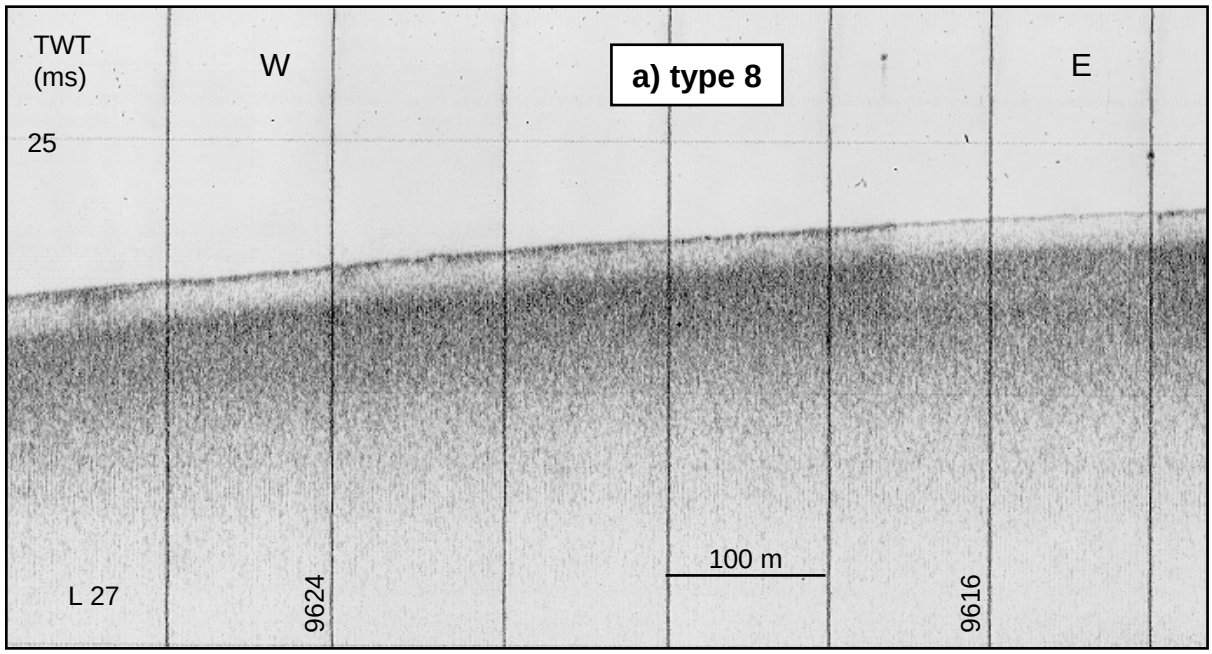
TWT
(ms)
W
a) type 8
E
25
100 m
L 27
9624
9616

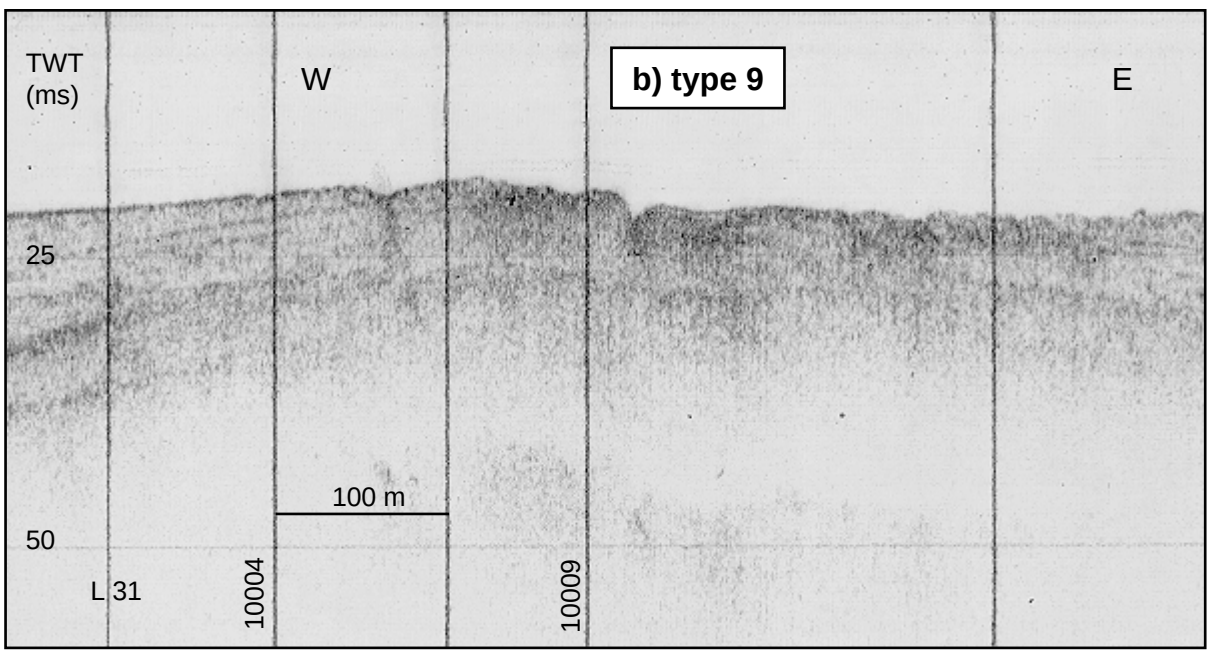
TWT
(ms)
W
b) type 9
E
25
100 m
50
L 31
10004
10009

Figure 8

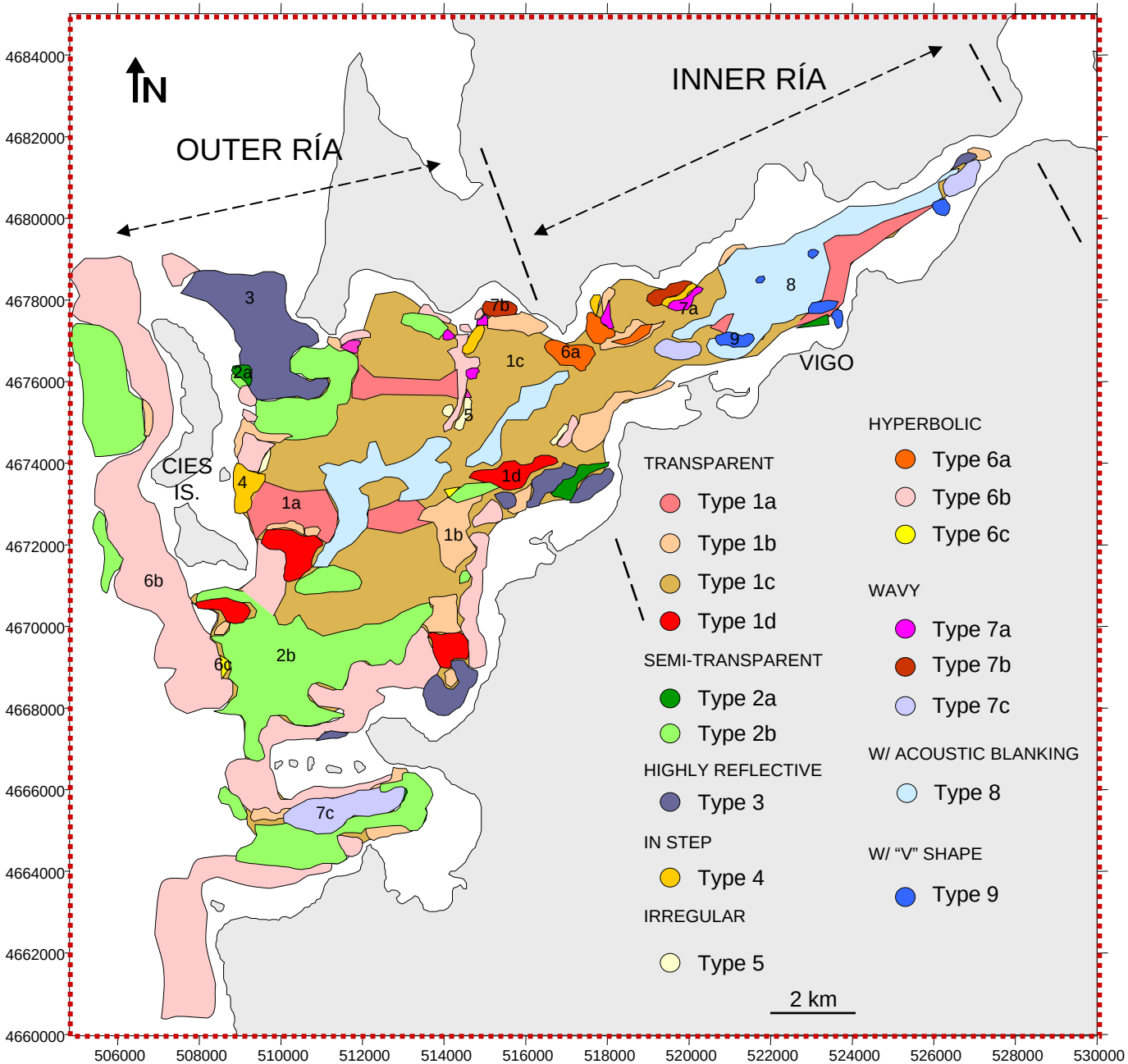
N
OUTER RÍA
INNER RÍA
VIGO
CIES
IS.
3
2a
4
1a
6b
6c
2b
7c
5
1c
7b
6a
1d
1b
7a
8
9
TRANSPARENT
Type 1a
Type 1b
Type 1c
Type 1d
SEMI-TRANSPARENT
Type 2a
Type 2b
HIGHLY REFLECTIVE
Type 3
IN STEP
Type 4
IRREGULAR
Type 5
HYPERBOLIC
Type 6a
Type 6b
Type 6c
WAVY
Type 7a
Type 7b
Type 7c
W/ ACOUSTIC BLANKING
Type 8
W/ "V" SHAPE
Type 9
2 km
4684000
4682000
4680000
4678000
4676000
4674000
4672000
4670000
4668000
4666000
4664000
4662000
4660000
506000
508000
510000
512000
514000
516000
518000
520000
522000
524000
526000
528000
530000

Figure 9

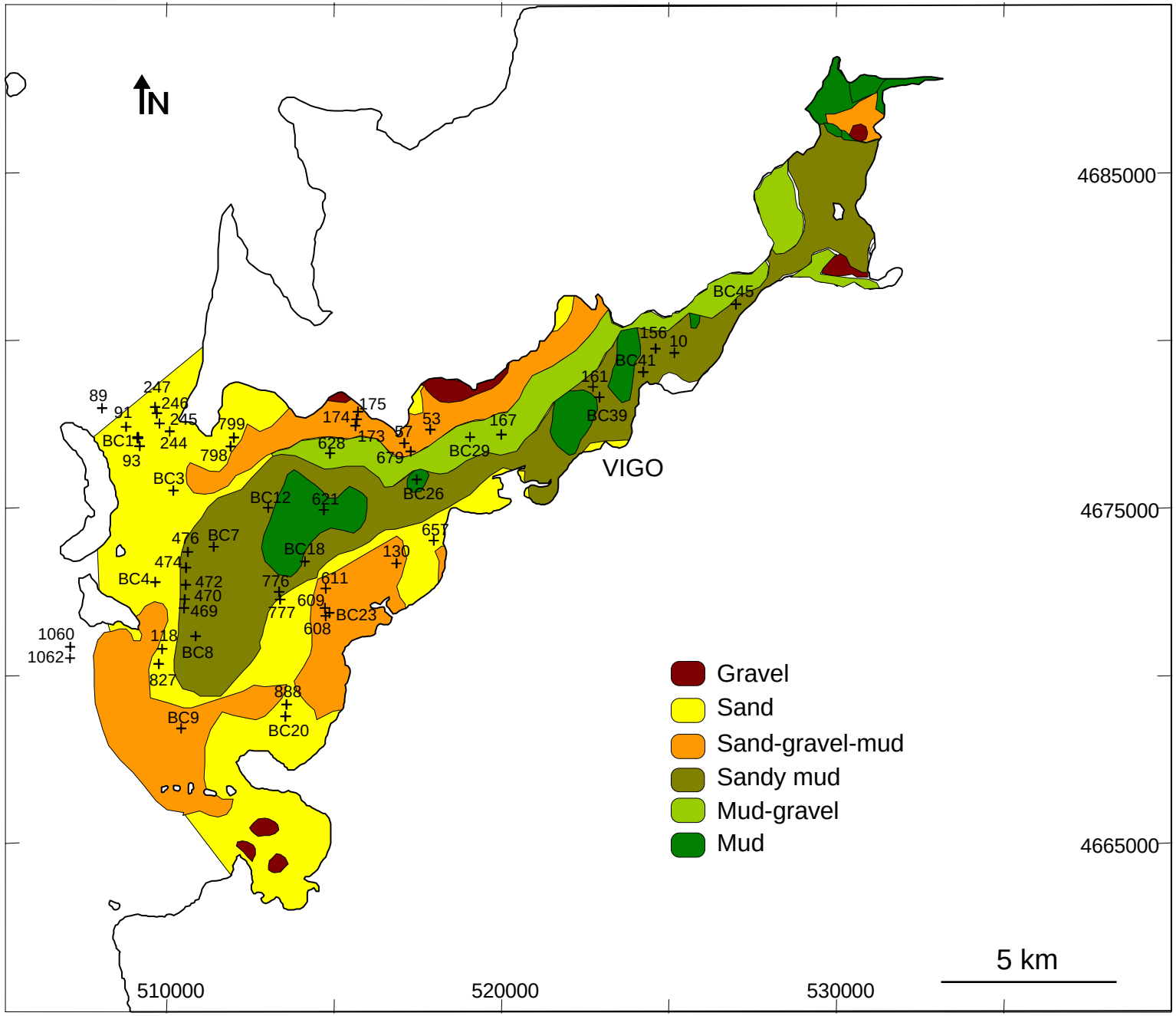
N
VIGO
4685000
4675000
4665000
510000
520000
530000
5 km
Gravel
Sand
Sand-gravel-mud
Sandy mud
Mud-gravel
Mud
BC45
156
10
BC41
161
BC39
167
53
175
174
57
173
628
679
BC29
799
798
247
246
245
244
89
91
93
BC3
BC12
621
BC26
476
BC7
474
BC4
472
470
469
BC18
130
657
776
611
609
777
BC23
608
1060
1062
118
BC8
827
888
BC9
BC20

Figure 10

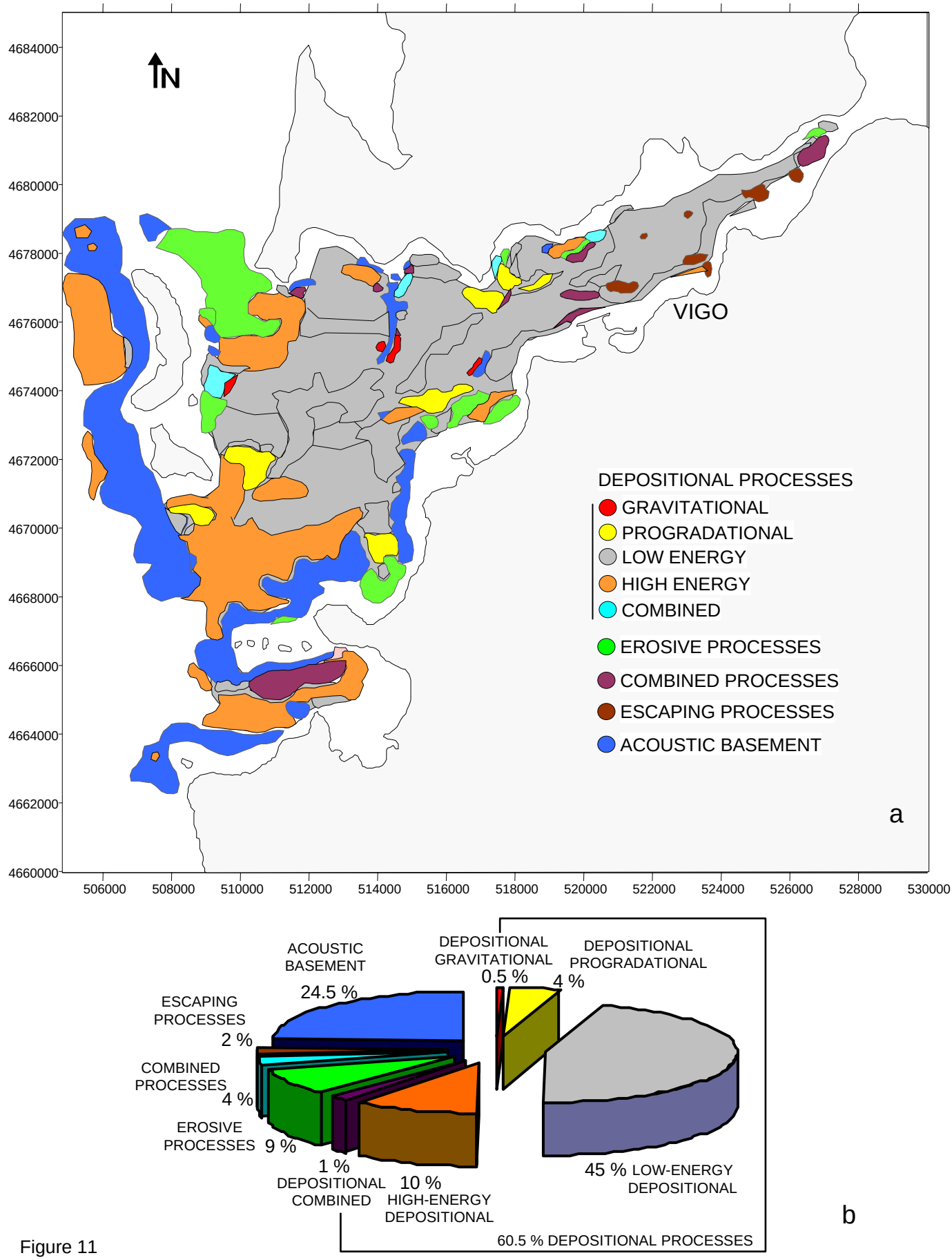
N
VIGO
DEPOSITIONAL PROCESSES
GRAVITATIONAL
PROGRADATIONAL
LOW ENERGY
HIGH ENERGY
COMBINED
EROSIVE PROCESSES
COMBINED PROCESSES
ESCAPING PROCESSES
ACOUSTIC BASEMENT
a
4684000
4682000
4680000
4678000
4676000
4674000
4672000
4670000
4668000
4666000
4664000
4662000
4660000
506000
508000
510000
512000
514000
516000
518000
520000
522000
524000
526000
528000
530000
ACOUSTIC BASEMENT
24.5 %
ESCAPING PROCESSES
2 %
COMBINED PROCESSES
4 %
EROSIVE PROCESSES
9 %
1 %
DEPOSITIONAL COMBINED
10 %
HIGH-ENERGY DEPOSITIONAL
DEPOSITIONAL GRAVITATIONAL
0.5 %
4 %
DEPOSITIONAL PROGRADATIONAL
45 %
LOW-ENERGY DEPOSITIONAL
60.5 % DEPOSITIONAL PROCESSES
b

Figure 11